

Analysis of Longitudinal Aerodynamic Characteristics of an Aircraft Model with and Without Winglet

Altab Hossain ^{a*}, Prithvi Raj Arora ^b, Ataur Rahman ^c, Abdul Aziz Jaafar ^b,
A.K.M. Parvez Iqbal ^a

^a Department of Mechanical Engineering, University Industry Selangor, Jln Timur Tambahan, 45600 Batang Berjuntai, Selangor Darul Ehsan, Malaysia

^b Department of Aerospace Engineering, University Putra Malaysia, Malaysia

^c Department of Mechanical Engineering, International Islamic University Malaysia

Abstract

This paper describes the influences of two pair of elliptical and circular shaped winglets with the wing of the aircraft model for the reduction of induced drag without increasing the span of the aircraft. Aerodynamic characteristics for the model aircraft wing with NACA section No. 65-3-218 with and without elliptical and circular winglets have been studied using a subsonic wind tunnel of 1m × 1m rectangular test section. Lift and drag measurements are carried out using a six component external balance. Tests are carried out on the aircraft model with and without winglet at the Reynolds numbers 0.17×10^6 , 0.21×10^6 and 0.25×10^6 . The experimental results show that lift curve slope increases by 1-6% with the addition of certain winglet configurations and at the same time, the drag decreases by 20-28% as compared to the aircraft model with and without winglet for the maximum Reynolds number considered in the present study. The experimental approach and a summary of the main findings are presented.

© 2008 Jordan Journal of Mechanical and Industrial Engineering. All rights reserved

Keywords: Winglet; Induced drag; External balance; Lift curve slope;

Nomenclature

α	: Angle-of-attack
D	: Drag force
L	: Lift force
ρ_∞	: Air density
S	: Reference area
V_∞	: Free stream velocity
a_0	: Lift slope
C_D	: Drag coefficient
C_L	: Lift coefficient
d	: Diameter of sphere
$[K_{ij}]$: Coefficient matrix

1. Introduction

For a number of years many investigations have been carried out to prove the possible benefits of modifying wing tip flow. The aerodynamic performance of an aircraft can be improved by a wingtip device which diffuses the

strong vortices produced at the tip and thereby optimise the span wise lift distribution, while maintaining the additional moments on the wing within certain limits. For this purpose the researchers have been doing experiments to produce favorable effects of the flow field using wing tip and reducing the strength of the trailing vortex with the aid of wingtip devices, e.g., winglets, wing tips of complex plan-form, sails, and various modifications of the wingtip side edge. The winglet is cambered and twisted so that the rotating vortex flow at the wing tip creates a lift force on the winglet.

From the beginning of aviation era, designers were searching for methods and technologies for reducing the required fuel consumption of the commercial aircraft. Wingtip devices aimed at the reduction of induced drag, which was responsible for 30-40% of the total drag of a transport-aircraft at long-range cruise condition and for considerably downgrading the climb performance of an aircraft [1]. Winglet alongside with tip tanks, raked wingtips, and aligned fans are belonged to this class of devices.

Modern interest in winglets spans the last 25 years. In July 1976, Richard Whitcomb of NASA Langley Research Centre published a general design approach that

* Corresponding author. e-mail: altab75@unisel.edu.my

summarized the aerodynamic technology involved in winglet design. Small and nearly vertical fins were installed on a KC-135A and flights were tested in 1979 and 1980 [2-3]. Whitcomb showed that winglets could increase an aircraft's range by as much as 7% at cruise speeds. A NASA contract [4] in the 1980s assessed winglets and other drag reduction devices, and they found that wingtip devices (winglet, feathers, sails, etc.) could reduce induced drag by 10 to 15% if they are designed as an integral part of the wing.

The "spiroid" wingtip [5] produces a reduction in induced drag at the same time blended winglet [6] reduces drag by eliminating the discontinuity between the wing tip and the winglet. A smoothed version is used on the gently upswept winglet of the Boeing 737-400. Boeing Business Jets and Aviation Partners, Inc. have embarked upon a cooperative program to market conventional winglets for retrofit to the Boeing 7xx series of jetliners. Flight tests on the Boeing Business Jet 737-400 resulted in a 7% drag reduction. Theoretical predictions had indicated that the configuration would have only a 1-2% improvement of drag reduction, and wind tunnel tests had shown only 2% drag reduction [7]. This indicates that wind tunnel test results of winglet configurations should be reviewed with some caution.

Jones [8] investigated the advantages of single winglets for small transport aircraft, on which they can provide 10% reduction in induced drag compared with elliptical wings. Winglets are being incorporated into most new transport aircraft, including the Gulf stream III and IV business jets [9], the Boeing 747-400 and McDonnell Douglas MD-11 airliners, and the McDonnell Douglas C-17 military transport. The first industry application of the winglet concept was in wingtip sail. The Pennsylvania State University (PSU) 94-097 airfoil has been designed for use on winglets of high-performance sailplanes [10]. To validate the design codes, as well as the design itself, the airfoil was tested in the Penn State Low-Speed, Low-Turbulence Wind Tunnel from Reynolds numbers of 0.24×10^6 to 1.0×10^6 . Performance predictions from two well-known computer codes are compared to the data obtained experimentally, and both are found to generate results that are in good agreement with the wind tunnel measurements.

J. J. Spillman at the Cranfield Institute of Technology in England [11] carried out another investigation on wing tip airfoils. He investigated the use of one to four sails on the wingtip fuel tank of a Paris MS 760 Trainer Aircraft. The flight test results confirmed the wind tunnel test results, demonstrated shorter takeoff rolls, and reduced fuel consumption [12]. Spillman later investigated wingtip vortex reduction due to wing tip sails, and found lower vortex energy 400-700 m behind the aircraft, although the rate of decay beyond that was somewhat lower [13].

There has been limited investigation of multiple winglets for aircraft. The split-tip design [14] by Heinz Klug for an aircraft wing is considered a primitive multiple winglets that was created to exploit the non-planar wake geometry by reducing induced drag and wing stress. A biologist with an aerodynamic background has done extensive investigation of the split wingtips of soaring birds and he demonstrated that the tip slots of soaring birds reduce induced drag and increase the span factor of the

wings [15]. He found remarkable improvements of slotted wingtips compared with conventional wing with a Clark Y airfoil and he investigated that with the same increase in angle of attack, the Clark Y airfoil tip increased the base wing drag by 25%, while the feathered tip actually reduced the drag by 6%.

To improve the performance of a wing, the multi-winglet [16] design was evaluated to demonstrate its advanced performance potential over the baseline wing and an equivalent single winglet. The results show that certain multi-winglet configurations reduced the wing induced drag and improved L/D by 15-30% compared with the NACA 0012 wing section. In Europe, an extension to the wing tip airfoils has been developed called Wing-Grid [17]. Wing-Grid is a set of multiple wing extensions added to the wing. These small wings are added at various angles so that their tip vortices do not interact to form a strong vortex. These smaller vortices dissipate the vortex energy so that the lift distribution is modified and the induced drag of the wing is reduced. However, this concept is limited, since it is not able to change configuration in flight to optimise drag reduction.

Aerodynamic characteristics for the aircraft model with and without winglet having wing with NACA section No. 65-3-218 has been presented in this paper. The study on the enhanced performance of the aircraft models is also given by incorporating elliptical and circular winglets. An interaction matrix method has also been presented to revalidate the calibration matrix data provided by the manufacturer of the six-component external balance. The calibration of free stream velocity and flow quality in the test section has been established and documented.

2. Methodology

2.1. Speed calibration

Subsonic wind tunnel of 2.5m length, 1m width and 1m height rectangular test section at the Aerodynamics Laboratory of the Aerospace Engineering Department, University Putra Malaysia is used for carrying out the experiments. The ambient pressure, temperature and humidity are recorded using barometer, thermometer, and hygrometer respectively for the evaluation of air density in the laboratory environment.

The RPM controller of the wind tunnel controls the airflow velocity. For the different Hz settings at the RPM controller, the flow velocities in wind tunnel test section are recorded using six-component external balance software. In addition to this dynamic pressure at the picot, tube is recorded with digital manometer and corresponding velocities are calculated [18] (see Table 1).

The validity of the digital manometer was confirmed by comparing the dynamic pressure measured through the digital manometer and through the tube manometer used along with the picot tube mounted in the test section. The flow velocity versus RPM controller speed curves is plotted for the data obtained through six components external balance software, digital manometer and tube manometer and are given in Fig. Least square fit lines are

drawn through the data and the corresponding lines are given in Fig.

Table 1: Speed calibration data

S. No.	Hz	Free stream flow velocity (m/s)		
		External balance software	Digital manometer	Manometer tube
1	0.0	0.00	0.00	0.00
2	3.0	1.93	2.21	2.70
3	5.0	3.87	3.69	4.04
4	7.5	6.40	6.72	6.67
5	10.0	9.07	9.42	9.30
6	12.5	11.60	12.06	12.07
7	15.0	14.03	14.76	14.77
8	17.5	16.50	17.35	17.42
9	20.0	18.83	20.08	20.15
10	22.5	21.17	22.65	22.82
11	25.0	23.50	25.17	25.45
12	27.5	25.80	27.65	28.00
13	30.0	27.93	30.20	30.41

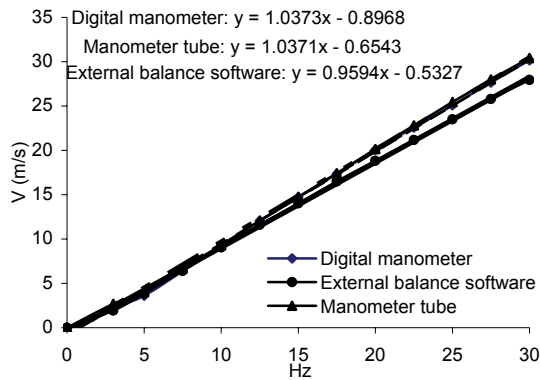


Figure 1: Free stream velocity versus RPM controller speed.

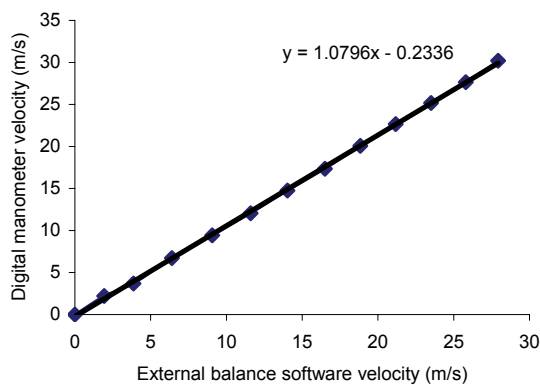


Figure 2: Flow velocity calibration for external balance

It is observed that the curves for the digital manometer and the tube manometer readings are practically the same whereas the curve for the data using six-component external balance software deviates a little from the other two curves. The experimental error using the external balance is nearly 6%. The flow velocity readings of the external balance are corrected through the following

calibration equation obtained through the data shown in Fig.,

$$y = 1.0796x - 0.2336 \tag{1}$$

Where x denotes external balance software velocity (m/s) and y denotes digital manometer velocity (m/s). Using the equation (1), the actual value of free stream air velocity will be 21.36 m/s for corresponding 20 m/s of air velocity from six-component external balance software.

2.2. Flow Uniformity

The dynamic pressure is measured using digital manometer at different locations in the test section (see Fig. 3) in YZ-plane by means of a picot tube for a RPM controller setting of 15 Hz. For different locations of the measurement grid, the experiments are repeated three times and the experimental data is given in Table 2. The average (mean) dynamic pressure is obtained from the measured dynamic pressure and is given in the last column of Table 2. The dynamic pressure variations from the mean are calculated in percentage at different locations of YZ-plane and are given in Table 3. Using these data, dynamic pressure variations from the mean (percentage) versus distance from wind tunnel floor (cm) are plotted in Figure 4. From figure-4 it is observed that the variation of dynamic pressure in the test section is within $\pm 0.5\%$ which indicates that there is very good uniformity of flow in the test section of the wind tunnel.

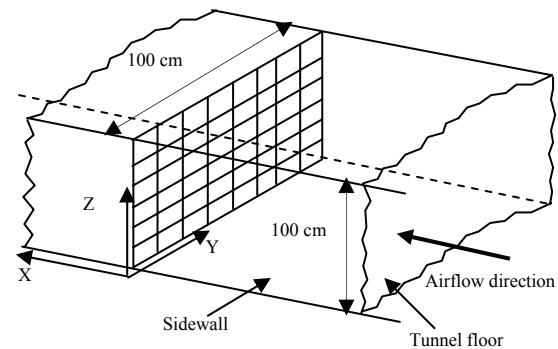


Figure 3: Schematic view of the wind tunnel test section

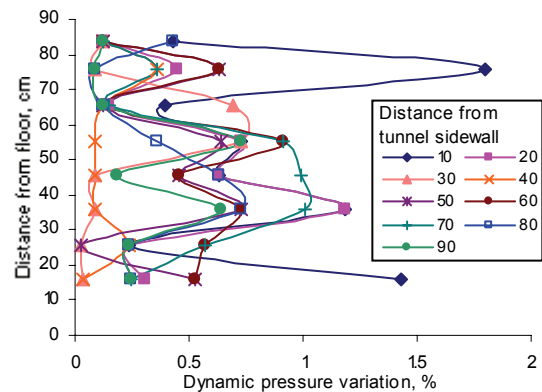


Figure 4: Dynamic pressure variation in the wind tunnel test section.

Table 2: Dynamic pressure at a cross section of the wind tunnel test section.

S. No	Z-axis (Down) [cm]	Dynamic pressure [Pa]									
		Distance from wall (Y-axis) [cm]									
		10	20	30	40	50	60	70	80	90	Mean
1	83.5	121.67	121.00	121.00	121.00	121.00	121.00	121.00	121.67	121.00	121.15
2	75.5	126.00	124.33	123.67	123.33	123.00	123.00	123.33	123.67	123.67	123.78
3	65.5	123.67	123.00	122.33	123.33	123.33	123.33	123.00	123.33	123.33	123.19
4	55.5	123.00	123.00	123.00	122.00	121.33	121.00	121.00	121.67	123.00	122.11
5	45.8	123.67	123.67	123.00	123.00	122.33	122.33	121.67	123.67	122.67	122.89
6	35.8	123.00	123.00	121.67	121.67	120.67	120.67	120.33	120.67	122.33	121.56
7	25.8	124.00	124.00	123.67	124.00	123.67	123.00	123.00	124.00	124.00	123.70
8	16.0	121.00	119.67	119.33	119.33	118.67	118.67	119.00	119.00	119.00	119.30

Table 3: Dynamic pressure variation at a cross section of the wind tunnel test section.

S. No	Z-axis (Down) [cm]	Dynamic pressure variation [%]									
		Distance from wall (Y-axis) [cm]									
		10	20	30	40	50	60	70	80	90	Mean
1	83.5	0.43	0.12	0.12	0.12	0.12	0.12	0.12	0.43	0.12	0.2
2	75.5	1.80	0.45	0.09	0.36	0.63	0.63	0.36	0.09	0.09	0.5
3	65.5	0.39	0.15	0.69	0.12	0.12	0.12	0.15	0.12	0.12	0.2
4	55.5	0.73	0.73	0.73	0.09	0.64	0.91	0.91	0.36	0.73	0.6
5	45.8	0.63	0.63	0.09	0.09	0.45	0.45	0.99	0.63	0.18	0.5
6	35.8	1.19	1.19	0.09	0.09	0.73	0.73	1.01	0.73	0.64	0.7
7	25.8	0.24	0.24	0.03	0.24	0.03	0.57	0.57	0.24	0.24	0.3
8	16.0	1.43	0.31	0.03	0.03	0.53	0.53	0.25	0.25	0.25	0.4

2.3. Wind Tunnel Model details and Instrumentation

The wind tunnel test aircraft model consists of rectangular wing with NACA section No. 65-3-218-aerofoil 0.66 m span and a 0.121 m chord. Two sets of elliptical and circular shaped winglets were designed of wood for the above wing. Figure-5 shows a photograph of the model aircraft with winglet, which is mounted horizontally in the test section of the wind tunnel.



Figure 5: Aircraft model check for 0° angle of attack.

The tests were carried out with free-stream velocities of 21.36 m/s, 26.76 m/s, and 32.15 m/s respectively with and without winglet of different configurations. The ambient pressure, temperature and humidity were recorded using barometer, thermometer, and hygrometer respectively for the evaluation of air density in the laboratory environment. Longitudinal tests were carried out at an angle of attack

ranging from zero degree to 14 degrees with an increment of 2 degrees. The coefficient of lift (Table 4), coefficient of drag (Table 5), the ratio of lift/drag (Table 6) and lift curve slopes data (Table 7) are obtained from the experimental results as per the procedure explained in [18-19].

2.4. Calibration of the Balance

Calibration of the six-component balance has been done to check the calibration matrix data provided by the manufacturer. Figure 6 shows a photograph of the calibration rig used for the validation of calibration matrix, which is mounted on the upper platform of the balance in place of model.

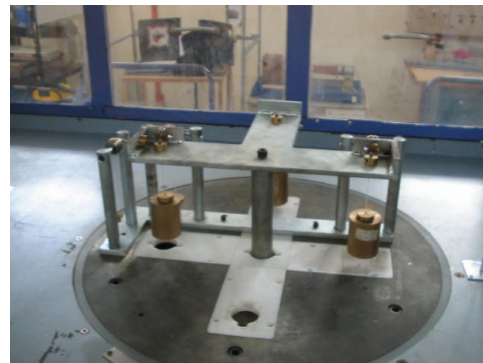


Figure 6: Calibration rig mounted on the floor of the wind tunnel test section

Table 4: Lift coefficients experimental data

S. No.	Winglet Configuration	Reynolds Number [10 ⁶]	Lift coefficient, C _L		
			Initial Angle of Attack [0°]	Stall Angle of Attack [8°]	Final Angle of Attack [14°]
1	Without Winglet	0.17	0.237	0.805	0.657
		0.21	0.259	0.817	0.584
		0.25	0.306	0.879	0.733
2	Elliptical Winglet, Configuration 1 (0° angle)	0.17	0.299	0.829	0.641
		0.21	0.327	0.889	0.700
		0.25	0.359	0.934	0.713
3	Elliptical Winglet, Configuration 2 (60° angle)	0.17	0.386	0.930	0.729
		0.21	0.394	0.934	0.815
		0.25	0.416	1.018	0.885
4	Circular Winglet, Configuration 1 (0° angle)	0.17	0.407	0.852	0.563
		0.21	0.429	0.908	0.7150
		0.25	0.430	0.967	0.775
5	Circular Winglet, Configuration 2 (60° angle)	0.17	0.436	0.939	0.775
		0.21	0.451	0.957	0.737
		0.25	0.487	0.985	0.823

Table 5: Drag coefficients experimental data

S. No.	Winglet Configuration	Reynolds Number [10 ⁶]	Drag coefficient, C _D		
			Initial Angle of Attack [0°]	Transition Angle of Attack [4°]	Final Angle of Attack [14°]
1	Without Winglet	0.17	0.085	0.104	0.249
		0.21	0.083	0.100	0.275
		0.25	0.065	0.085	0.211
2	Elliptical Winglet, Configuration 1 (0° angle)	0.17	0.053	0.058	0.136
		0.21	0.050	0.056	0.140
		0.25	0.049	0.053	0.128
3	Elliptical Winglet, Configuration 2 (60° angle)	0.17	0.070	0.078	0.166
		0.21	0.058	0.065	0.153
		0.25	0.047	0.060	0.134
4	Circular Winglet, Configuration 1 (0° angle)	0.17	0.057	0.063	0.186
		0.21	0.053	0.057	0.154
		0.25	0.052	0.055	0.130
5	Circular Winglet, Configuration 2 (60° angle)	0.17	0.075	0.092	0.192
		0.21	0.063	0.083	0.172
		0.25	0.050	0.069	0.158

Table 6: Lift/Drag Ratio experimental data

S. No.	Winglet Configuration	Reynolds Number [10 ⁶]	Lift/Drag ratio [L/D]			
			Initial Angle of Attack [0°]	Transition Angle of Attack [4°]	Transition Angle of Attack [6°]	Final Angle of Attack [14°]
1	Without Winglet	0.17	2.8	5.7	5.7	2.6
		0.21	3.1	6.1	5.9	2.1
		0.25	4.7	7.71	7.0	3.5
2	Elliptical Winglet, Configuration 1 (0° angle)	0.17	5.61	11.27	11.09	4.73
		0.21	6.53	12.30	11.84	5.02
		0.25	7.33	13.73	13.19	5.55
3	Elliptical Winglet, Configuration 2 (60° angle)	0.17	5.5	8.8	9.3	4.4
		0.21	6.7	10.8	11.4	5.3
		0.25	8.8	13.0	13.5	6.6
4	Circular Winglet, Configuration 1 (0° angle)	0.17	7.18	10.51	10.2	3.02
		0.21	8.02	11.96	11.6	4.65
		0.25	8.29	13.57	12.9	5.98
5	Circular Winglet, Configuration 2 (60° angle)	0.17	5.8	8.5	9.1	4.0
		0.21	7.1	9.5	10.1	4.3
		0.25	9.6	11.8	12.2	5.2

Table 7: Lift curve slopes data

S. No.	Free stream velocity [m/s]	Reynolds Number [10 ⁶]	Lift curve slopes				
			Without Winglet	Elliptical Winglet at [0°]	Elliptical Winglet at [60°]	Circular Winglet at [0°]	Circular Winglet at [60°]
1	21.36	0.17	3.72	3.83	3.85	3.77	3.76
2	26.76	0.21	4.01	4.09	4.13	4.03	3.96
3	32.15	0.25	4.11	4.15	4.36	3.93	3.67

The relationship between signal readings, L_i and the loads, F_i applied on the calibration rig are given by the following matrix equation, the detailed procedure of calibration is explained elsewhere [18-19]

$$\{L_i\} = [K_{ij}] \{F_i\} \quad (2)$$

Where $[K_{ij}]$ is the coefficient matrix, $\{L_i\}$ is the signal matrix, $\{F_i\}$ is the load matrix.

The calibration matrix is obtained by finding the inverse of K_{ij} , coefficient matrix and it compares well (2% error) with the calibration matrix data supplied by the manufacturer with six component external balance [19].

2.5. Verification of Wind Tunnel Measurements with Sphere

The force measurements, using a sphere model, were carried out in 1m × 1m low speed open wind tunnel described in the previous section. Figure 7 shows the photograph of a sphere mounted through the strut over the platform of the six-component balance placed in the wind tunnel section. The tests were conducted for free-stream velocities of 5.16 m/s, 10.56 m/s, 15.96 m/s, and 21.36 m/s, respectively (Table 8).



Figure 7: Sphere model mounted in wind tunnel test section

Table 8: Experimental data with sphere

S. No.	Free stream velocity [m/s]	Reynolds number	Drag Force [N]	Drag Coefficient	
				Experiment	Experimental (Schlichting [20])
1	5.16	3.3×10^4	0.051	0.404	0.400
2	10.56	6.8×10^4	0.23	0.436	0.480
3	15.96	1.0×10^5	0.45	0.374	0.430
4	21.36	1.4×10^5	0.66	0.306	0.410

For each free stream conditions drag force was obtained using a computerized data acquisition system and coefficient of drag (Table 8) is calculated using the Eq. (3) [20] given below,

$$C_D = \frac{D}{\frac{1}{2} \rho_{\infty} V_{\infty}^2 S} \quad (3)$$

Where D is the drag force, ρ_{∞} is the air density, V_{∞} is the free stream velocity, and S is the frontal area of sphere

defined by $S = \frac{\pi d^2}{4}$, where d is the nominal diameter of the sphere.

The coefficient of drag for a sphere as a function of the Reynolds number obtained from the book [21] is given in Table 8. The drag coefficient characteristics for a sphere, as reported in [21], are presented with the drag coefficients under the test as a function of the Reynolds number in Figure 8. From the graph, it is observed that C_D variations are qualitatively similar; both with a decrease in C_D near a critical Reynolds number of 3×10^5 , coinciding with natural transition from laminar to turbulent flow. For the reference data of sphere, C_D is about 0.4 in the Reynolds number range below the critical value and drops to about 0.1 for Reynolds numbers above the critical value. When the critical Reynolds number (i.e., the boundary layer separation) is exceeded, transition takes place on the front face, the boundary layer around the sphere becomes turbulent and the coefficient of drag is significantly reduced as the separation point on the boundary layers moves back [22]. This experiment verifies the measurements in wind tunnel compared with the data as reported in [21].

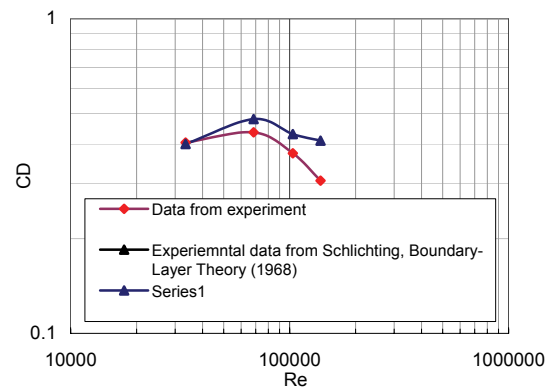


Figure 8: Drag coefficient versus Reynolds number for the sphere model

3. Results and Discussions

Wind-tunnel measurements using the aircraft model without winglet and with winglet of different configurations as configuration 1 (Winglet inclination at 0°), and configuration 2 (Winglet inclination at 60°) were done at Reynolds numbers 0.17×10^6 , 0.21×10^6 and 0.25×10^6 . The coefficient of lift and coefficient of drag are calculated from the experimental results as per the procedure explained in [18-19].

3.1. Lift Coefficient Characteristics

The coefficient of lift versus angle of attack for the aircraft model with and without winglet studied in Figure 9 for the present investigation are shown in Figure 9 for the maximum Reynolds number of 0.25×10^6 . From Figure 9, it is observed that the lift increases with increase in angle of attack to a maximum value and thereby decreases with further increase in angle of attack. The initial values of lift coefficient occur at zero angle of attack and the maximum

values of the lift coefficient occur at an angle of attack of 8 degrees. Above this angle of attack, lift curve begins to decrease with further increase in angle of attack. The reason for a drop in lift coefficient beyond 8-degree angle of attack is probably due to the flow separation, which occurs over the wing surface instead of having a streamlined laminar flow there. The stalling angle happens to be approximately 8° for all the Reynolds numbers under the present study. The least square fit lines are drawn through the data obtained for different configurations until angle of attack of 8° and the lift curve slopes, $\frac{dC_L}{d\alpha}$ are found as 4.11, 4.15, 4.36, 3.93, and 3.67 respectively. It is observed that the $\frac{dC_L}{d\alpha}$ slope for all the configuration is practically same with only a marginally high slope, a_0 for elliptical winglet of configuration 1 and 2 as compared to the circular winglet and without winglet configuration. The other details of the lift coefficients are given in Table 4.

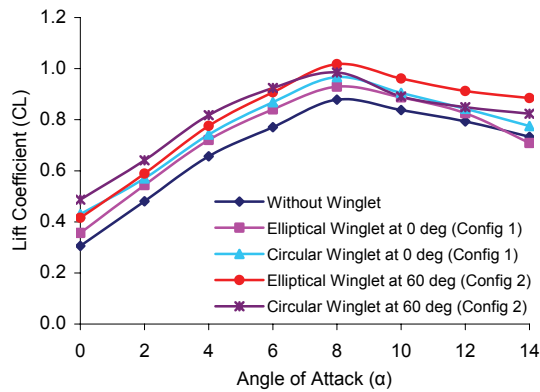


Figure 9: Lift Coefficients for the Aircraft Model

3.2. Drag Coefficient Characteristics

From Figure 10, it is observed that the drag coefficient for the aircraft model measured under all the configurations under this study shows an increasing trend with angle of attack for a Reynolds number 0.25×10^6 . The drag increases slowly with increase in angle of attack to a certain value and then it increases rapidly with further increase in angle of attack. The rapid increase in drag coefficient, which occurs at higher values of angle of attack, is probably due to the increasing region of separated flow over the wing surface, which creates a large pressure drag. From Figure 10 it is observed that the values of the minimum drag coefficients are 0.065, 0.049, 0.047, 0.052, and 0.050 respectively for different configurations for the maximum Reynolds number of 0.25×10^6 that occur at zero angle of attack. In particular, the measured drag against the angle of attack is minimum for the elliptical winglet of configuration 1 and 2 over the values of the range of angle of attack considered under this study. The measured drag values for the aircraft model with circular winglet of configuration 1 are also practically same as compared to the elliptical winglet. To establish the superiority of the elliptical winglet over the circular winglet experiments that are more detailed are required.

The other details of the drag coefficients are given in Table 5.

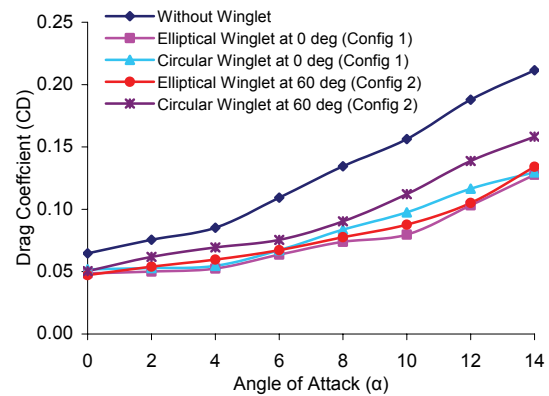


Figure 10: Drag Coefficients for the Aircraft model

3.3. Lift/Drag Ratio Characteristics

The lift/drag ratio is the outcome of the observations made in the two preceding sections. It is observed from Figure 11 that the lift/drag ratio for all the configurations considered increases with an angle of attack to its maximum value and thereby it decreases with further increase in angle of attack for a Reynolds number 0.25×10^6 . In particular, it is observed that the maximum lift/drag ratio for all the configurations considered in the study falls in the range of 4 to 6 degrees of angle of attack. The aircraft model without winglet gives a measured lift/drag ratio of 7.71 whereas the respective values of the lift/drag ratio for the different configurations are 13.73, 13.0, 13.57, and 11.77 respectively at an angle of attack of 4° . The lift/drag ratio values for the angle of attack of 6° are 7.0, 13.19, 13.48, 12.90, and 12.25 respectively for the different configurations. Practically it is observed that the lift/drag ratio versus angle of attack curve gives similar results for 4 to 8 degrees, for the elliptical winglet of configuration 1, elliptical winglet of configuration 2, and for circular winglet of configuration 1. The other details of the lift/drag ratio at other angle of attacks are given in Table 6 considered in the study.

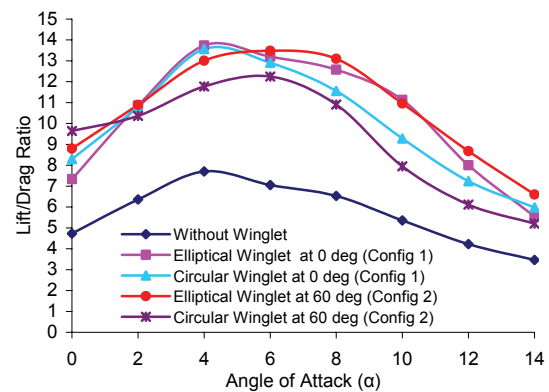


Figure 11: Lift/Drag Ratio for the Aircraft model

From Figure 9 and 10, it is observed that the lift curve slope increases with the addition of the winglet (Winglets

inclination at 60^0 and 0^0 ranging from 1% to 6% (Table 7) and at the same time the drag decreases for the addition of winglet ranging from 20% to 28% at the maximum Reynolds number of 0.25×10^6 . These experimental results can be explained by comparing with the results obtained at the Georgia Institute of Technology [16]. The tests were run in three configurations: winglets off (Configuration 0), winglets installed at zero degrees (Configuration 1), and winglets deployed at $+20^0$, $+10^0$, 0^0 , -10^0 , -20^0 (Configuration 2). They showed that flat plate winglets set at zero degrees (Configuration 1) increased lift curve slope by 10% for the maximum Reynolds number of 0.29×10^6 . They also showed that configuration 2 provided the largest increase of lift curve slope, ranging from 15% to 22% increases.

From this investigation it is observed that at the maximum Reynolds number of 0.25×10^6 elliptical winglet of configuration 1 and 2 (Figure 9) provides the largest increase of lift curve slope, ranging from 1% to 6% increases and at the same time drag decreases more for these two configurations ranging from 24.6% to 28% decrease, giving an edge over other configurations as far as L/D for the elliptical winglet of configuration 1 and 2 (Figure 11) is considered. Decisively it can be said that the elliptical winglet of configuration 2 (Winglets inclination at 60^0) has the better performance giving about 6% increase of lift curve slope as compared to other configurations and it is giving the better lift/drag ratio (13.5). Full results of the studies on lift coefficient, drag coefficient and lift/drag ratio can be found in Reference [18].

4. Conclusions

Following are the conclusions drawn from this investigation. The calibration matrix obtained through the interaction matrix method compares well with the matrix data as supplied by the manufactures of the six-component balance. Aerodynamic characteristics for the aircraft model with and without winglet having NACA wing No. 65-3-218 have been presented. Elliptical winglet at 60-degree incidence has the better performance giving about 6% increase in lift curve slope and thereby produces more lift and at the same time the drag decreases by 28% as compared to other configurations and it is giving the best lift/drag ratio for the maximum Reynolds number considered in the present study.

Acknowledgements

The authors are grateful for the support provided by grants from the IRPA (Project No: 09-02-04-0446-EA001), and the Aerodynamics Laboratory of Aerospace Engineering Department of the University Putra Malaysia for using the Wind Tunnel.

References

- [1] Bento, S.de, M.; Antonini P. Macedo and Dural H. da Silva F. "Considerations about Winglet Design". AIAA Paper 2003-3502.
- [2] Whitcomb, R. T. "A Design Approach and Selected Wind-Tunnel Results at High Subsonic Speeds for Wing-Tip Mounted Winglets". NASA TN D-8260, 1976.
- [3] Whitcomb, R. T. "Methods for Reducing Aerodynamic Drag". NASA Conference Publication 2211, Proceedings of Dryden Symposium, Edwards, California, 1981.
- [4] Yates, J. E., and C. Donaldson. "Fundamental Study of Drag and an Assessment of Conventional Drag-Due-To-Lift Reduction Devices". NASA Contract Rep 4004, 1986.
- [5] Louis, B. Gratzler. "Spiroid-Tipped Wing". U. S. Patent 5, 102068, 1992.
- [6] Reginald, V. French. "Vortex Reducing Wing Tip". U. S. Patent 4, 108403, 1978.
- [7] Clark, J. Aviation Partners, Inc., personal communication, 1999.
- [8] Jones, R. T. "Improving the Efficiency of Smaller Transport Aircraft". 14th Congress of the International Council of the Aeronautical Sciences, proceeding, Vol. 1, Toulouse, France, 1984.
- [9] Chandrasekharan, Reuben M., Murphy, William R., Taverna, Frank P., and Boppe, Charles W. "Computational Aerodynamic Design of the Gulfstream IV Wing". AIAA-85-0427, 1985.
- [10] Maughmer, M. D., S. S. Timothy., and S. M. Willits. "The Design and Testing of a Winglet Airfoil for Low-Speed Aircraft". AIAA Paper 2001-2478, 2001.
- [11] Spillman, J. J. "The use of wing tip sails to reduce vortex drag". Aeronautical Journal, Vol. 16, 1978, 387-395
- [12] Spillman, J. J., Ratcliffe, H. Y., and McVitie, A. "Flight experiments to evaluate the effect of wing-tip sails on fuel consumption and handling characteristics". Aeronautical Journal, Vol. 17, 1979, 279-281.
- [13] Spillman, J. J., and Fell, M. J. "The effects of wing tip devices on (a) the performance of the Bae Jetstream (b) the far-field wake of a Paris Aircraft". Paper 31A, AGARD CP No. 342, Aerodynamics of Vortical Type Flows in Three Dimensions, April, 1983, 31A-1-11
- [14] Heinz G. Klug. "Auxiliary Wing Tips for an Aircraft". U. S. Patent 4722499, February 1988.
- [15] Vance A.T. "Gliding Birds: Reduction of Induced Drag by Wing Tip Slots between the Primary Feathers". Journal of Experimental Biology, Vol. 180, No.1, 1993, 285-310
- [16] Smith, M. J., N. Komerath., R. Ames., O. Wong., and J. Pearson. "Performance Analysis of a Wing with Multiple Winglets". AIAA Paper-2001-2407, 2001.
- [17] Roche La. U., and Palffy S., "WING-GRID, a Novel Device for Reduction of Induced Drag on Wings," Proceedings of ICAS 96, Sorrento, 1996.
- [18] Hossain, A. "Investigations of Longitudinal Aerodynamic Characteristics of Aircraft Model with and without Winglet". M.Sc. Thesis, Department of Aerospace Engineering, Faculty of Engineering, Universiti Putra Malaysia, UPM Serdang, Selangor DE, Malaysia, 2005.
- [19] Prithvi, R. A., A. Hossain, A. A. Jaafar, P. Edi, T. S. Younis, and M. Saleem. "Drag Reduction in Aircraft Model using Elliptical Winglet". Journal of IEM, Malaysia, Vol. 66, No. 4, 2005, 1-8.
- [20] Bertin, John J., Aerodynamics for Engineers, Prentice-Hall, Inc, New Jersey, USA, 2002.
- [21] Schlichting, H. Boundary Layer Theory, McGraw-Hill Book Company, New York, USA, 1968.
- [22] Anderson, John. D, Introduction to Flight, McGraw-Hill Book Company, New York, USA, 2005.